Passive A-Band Wind Sounder (PAWS) for Measuring Tropospheric Wind Velocity

Shane Roark, Robert Pierce, Philip Slaymaker, Grzegorz Miecznik, Brian Johnson, Pei Huang, and Paul Kaptchen

Ball Aerospace & Technologies Corporation
1600 Commerce Street
Boulder, Colorado, 80306-1062

***Abstract*–The Passive A-Band Wind Sounder (PAWS) was funded through NASA's Instrument Incubator Program (IIP) to determine the feasibility of measuring tropospheric wind speed profiles from Doppler shifts in oxygen absorption lines. Although this passive approach is not expected to provide the potential performance of Doppler lidar, it is being pursued as a low-cost and low-risk alternative capable of providing better wind data than is currently available. The instrument concept is adapted from the Wind Imaging Interferometer (WINDII) sensor on the Upper Atmosphere Research Satellite. The operational concept for PAWS is to view an atmospheric limb over an altitude range from the surface to 20 km with a wide-field Doppler interferometer in a sun-synchronous low-earth orbit. Two orthogonal views of the same air mass will be used to resolve horizontal winds from measured line-of-sight winds.**

A breadboard instrument was developed to demonstrate the measurement approach and to optimize the design parameters for the subsequent engineering unit and future flight sensor. The breadboard instrument consists of a telescope, collimator, filter assembly, and Michelson interferometer. From interference between two tilted wavefronts, a fringe pattern is recorded on a sensitive CCD in order to determine the Doppler shift of the oxygen absorption line. This paper will describe the measurement approach and breadboard system, as well as radiative transfer and instrument model development.

I. Introduction

Measurement of global tropospheric wind profile is important for improving weather forecasting and understanding atmospheric transport and mixing of chemical and aerosol species. Wind speed and direction, as well as temperature, humidity, and pressure, are determined twice daily as a function of altitude using weather balloons with radiosondes that can be tracked as the balloon ascends through the atmosphere. This approach provides good local information about wind; however, weather balloons around the world collectively only probe a small fraction of the desired global coverage and do not retrieve any information about winds over the oceans. Satellite observations can provide ocean and global coverage by monitoring the movement of clouds and waves to determine wind speed and direction. The limitation with these approaches is that they cannot measure winds as a function of altitude throughout the atmosphere. Computer models routinely are used to estimate global winds based on satellite data of other atmospheric parameters, such as temperature and humidity. Although these models generate very good wind approximations, direct global measurement of wind speed and direction as a function of altitude in the troposphere would provide new information and detail for understanding atmospheric dynamics, including the processes that affect climate, weather, natural hazards, and transportation of pollutants. According to the recent NRC Decadal Survey, tropospheric winds are the number one unmet measurement objective for improving weather forecasts [1].

The Passive A-Band Wind Sounder (PAWS) was one of 23 proposals selected under NASA's Instrument Incubator Program (IIP) in 2004. The objective for PAWS is to determine the feasibility of measuring tropospheric wind speed profiles from Doppler shifts in oxygen absorption features. PAWS is a daytime-only approach and will not provide the level of accuracy, precision, or spatial coverage that is anticipated for Doppler lidar. However, PAWS does have the potential to provide much better wind data than is available in the near term with significantly lower cost, risk, and platform requirements than lidar. The PAWS instrument is small and lightweight, does not have any mechanisms for pointing or scanning, and the components have proven space heritage. Because the signal comes from scattered sunlight, PAWS does not require a powerful and reliable laser, high-speed detector, or any high-power or high-voltage components. Unlike lidar, the signal is insensitive to spacecraft altitude and PAWS can operate at 833 km as well as lower altitudes. The challenge for PAWS is not in development of the individual components, but rather to determine if the components can function collectively to provide the desired wind-profile data using the oxygen A-band.

The first year of the PAWS project was directed at designing and building a breadboard instrument and developing radiative transfer and instrument models. PAWS is now in its second year of funding and the focus is on using the breadboard instrument to demonstrate the measurement concept and identify the preferred instrument parameters for the subsequent engineering model. This paper will describe the measurement approach and construction of the breadboard system, and provide a brief overview of radiative transfer and instrument model development.

II. Operation Concept and Measurement Approach

The baseline on-orbit operational concept for PAWS is summarized in Fig. 1 and was derived from the Wind Imaging Interferometer (WINDII) on the Upper Atmosphere Research Satellite (UARS) [2]. From low-Earth orbit (LEO), the instrument views a one-dimensional atmospheric column from the ground to 20 km in elevation. The 20-km atmospheric limb is resolved into individual 1-km elements to obtain the line-of-site wind vectors as a function of altitude. The horizontal limb dimension will be set by the measurement integration time, which will be determined experimentally. For a baseline integration time of 30 seconds and a spacecraft ground speed of approximately 7 km/s, the width of the atmospheric column would be roughly 210 km. As shown in Fig. 2, the instrument will have fixed forward (FOV1) and rearward (FOV2) fields of view that are imaged simultaneously. The fields of view are oriented near 45° and 135° with respect to the spacecraft ground track to obtain the orthogonal horizontal wind vectors for each sampling volume. With this approach, there is a time lag of several minutes between the two spacecraft positions required to obtain the orthogonal wind vectors within the sample volume.

Since PAWS is a passive instrument, the spectral radiance along the entire line of sight is measured. Therefore, the data for a given altitude are contaminated by data from higher altitudes at other positions along the line of sight. There are two factors that reduce the significance of this complication. First, for a given tangent line of sight, the optical path is relatively short through the higher altitude shells of the atmosphere and the density of oxygen decreases with altitude, so the contribution to the absorption spectrum is relatively small. Second, at the near and far ends of the tangent line where higher altitudes are inadvertently sampled, the line of sight is not horizontal with respect to the Earth surface, so the magnitude of the wind vector is reduced.

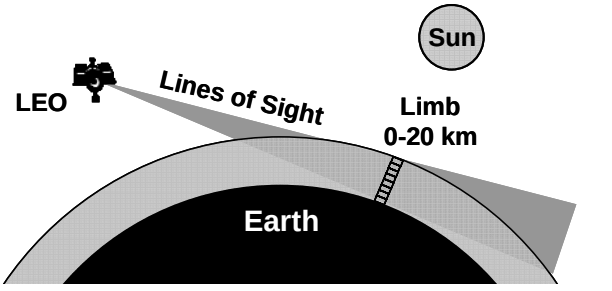

Fig. 1. Side view showing the on-orbit operation concept.

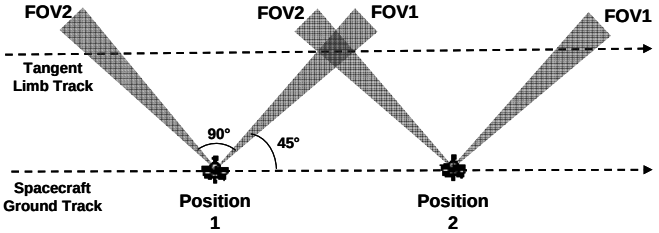

Fig. 2. Plan view showing the approach for measuring orthogonal wind vectors.

Fig. 3 shows a portion of the P-branch of the oxygen A-band spectrum, which results from (0←0) vibrational levels of the molecular $b^1\Sigma_g^+ \leftarrow X^3\Sigma_g^-$ electronic transition [3]. The oxygen A-band was selected for passive Doppler measurements because (1) the lines are not near or overlapping other features in the atmospheric absorption spectrum, (2) the lines are extremely sharp and well-resolved, (3) a wide range of line absorption depths are available to optimize the signal to noise ratio (SNR), (4) the tracer molecule is abundant and uniformly distributed in the troposphere, and (5) the A-band is in a spectral region compatible with high-spectral-resolution technology and silicon detectors with high quantum efficiency.

The baseline filtering approach for PAWS is to isolate a single absorption feature from the A-band spectrum. The filter function is shown in Fig. 3 overlapping with the specific line selected for baseline development of the PAWS breadboard. The resulting narrow-band spectrum collected through the filter is shown in Fig. 4. To illustrate the concept, spectra for a zero-wind (solid line) and greatly exaggerated Doppler-shifted wind (dashed line) are overlaid in the figure. The Doppler frequency shift, $\delta\nu$, is expressed

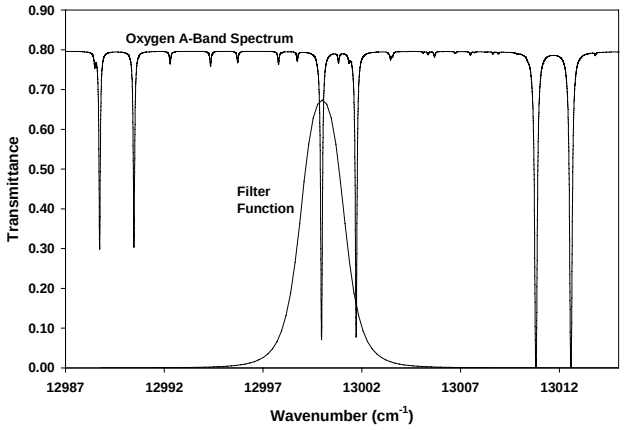

Fig. 3. A portion of the oxygen A-band spectrum showing the position of the filter function.

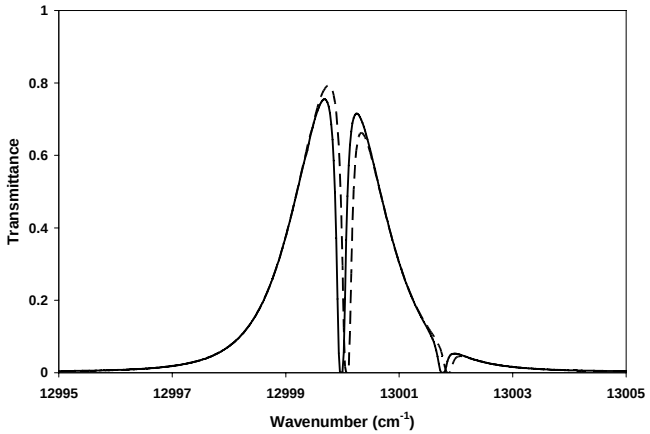

Fig. 4. Narrow-band absorption spectrum obtained through the filter for a zero-wind (solid line) and Doppler-shifted wind signal (dashed line).

as a function of the component of wind velocity in the direction of the instrument, υ_w, according to [4],

$$\delta\nu = \nu_0 \frac{\upsilon_w}{c}, \tag{1}$$

where ν_0 is the zero-wind absorption line center and c is the speed of light. From this relationship, a 5-m/s wind speed would only shift the 13,000 cm^{-1} absorbance line center by about 10^{-4} cm^{-1} or 10^{-6} nm, which would not be resolvable by a grating spectrograph. However, when the filtered light is passed through a Michelson interferometer, the Doppler shift in the phase of the modulation of the interferogram, $\delta\phi$, is dependent on the optical path difference, OPD, in the interferometer according to [4],

$$\frac{\delta\phi}{2\pi} = (\mathrm{OPD})\nu_0 \frac{\upsilon_w}{c} \tag{2}$$

Therefore, a large OPD can be used to accentuate the wind-induced frequency shift by measuring the phase shift of high-order fringes in the interferogram. Using this approach with a 3-cm OPD, the phase shift for the 13,000 cm^{-1} absorption line would be about 0.5 nm for the same 5-m/s wind speed. The tradeoff is that the visibility of the interferogram decreases as the OPD increases, so a compromise must reached to optimize the sensitivity of the measurement. Performing this trade study is one of the main goals for the breadboard instrument.

The instrument measurement concept for a single field of view is illustrated in Fig. 5. Scattered light from the entire 20-km atmospheric column is collected by the telescope, collimated, and filtered to isolate the desired absorption feature. The filtered light enters the interferometer and is split between two optical paths with unequal lengths. The beams are reflected by the mirrors, recombined at the beam splitter, and focused onto a two-dimensional detector array. In one of the optical path arms, the mirror is tilted so that the OPD between the two arms varies slightly and the interferogram is projected spatially across the detector. The

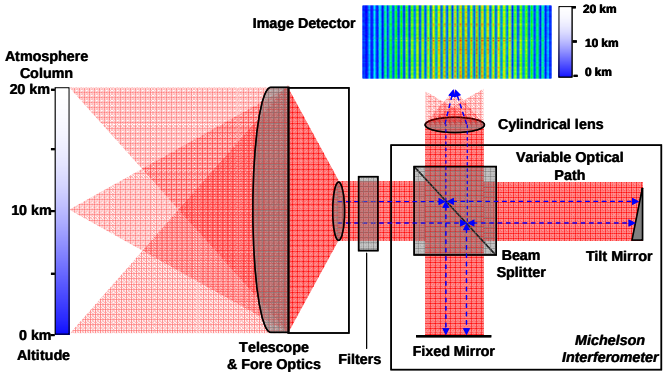

Fig. 5. PAWS instrument measurement concept.

interferograms from each 1-km segment of the atmospheric column are imaged simultaneously at different positions on the detector. Phase shifts relative to a zero-wind calibration source are determined by comparing the output at designated positions on the detector that span one or more periods or fringes of the interferograms.

III. Breadboard Instrument Development

The heart of the breadboard instrument is an interferometer, which is used to convert small wind-induced Doppler frequency shifts of the oxygen absorption line into phase shifts. The objectives for development of the breadboard system are to (1) clarify the problems associated with measuring phase shifts in an absorption line as apposed to an emission line, (2) identify and perform the trades that are needed to accomplish the measurement task, and (3) define the requirements for the subsequent engineering model. The breadboard is being used as a path-finding tool and must sacrifice some stability in order to accommodate a number of possible orientations and measurement schemes. For example, the filters and OPD must be adjustable to investigate different filtering approaches and achieve the best compromise between phase shift and interferogram visibility.

Photographs of the breadboard system are shown in Fig. 6, and a diagram is shown in Fig. 7. The main components are the telescope, a filter section, the interferometer, the

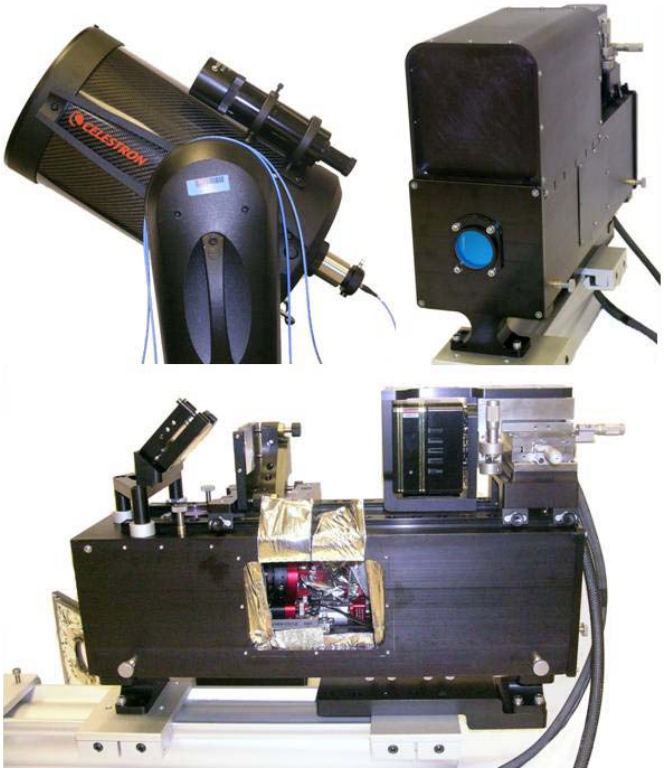

Fig. 6. Photographs of the PAWS breadboard system showing the telescope (top left), enclosed interferometer (top right), and side view of the opened interferometer.

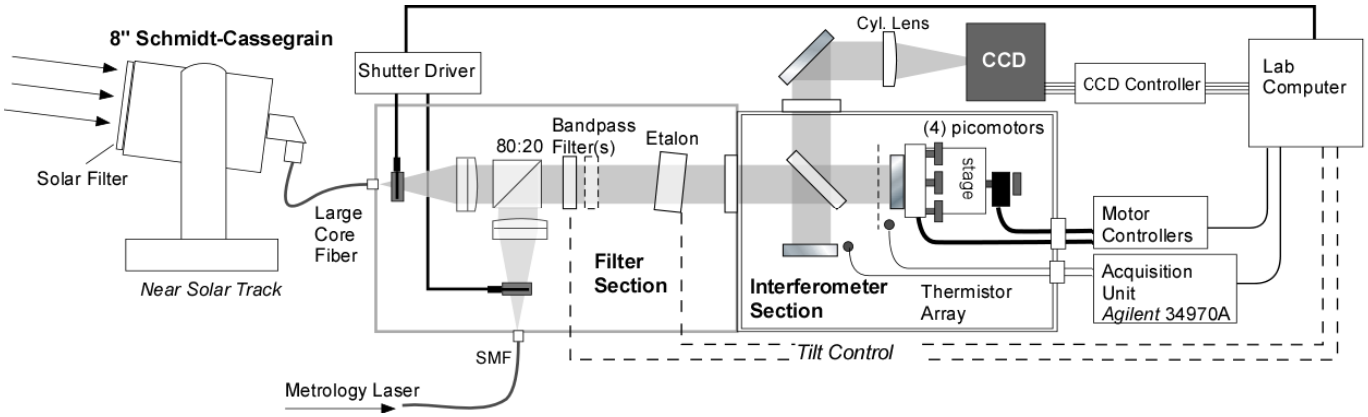

Fig. 7. Schematic diagram of the PAWS breadboard system.

detector and supporting electronics. The telescope is an eight-inch Schmidt-Cassegrain, and is used to only to gather light from the full field of view (*i.e.,* it is single channel). Since the Michelson is tolerant to light sources with low spatial coherence, the telescope is conveniently fiber coupled to the interferometer using a large-core optical fiber. This arrangement allows the telescope to be pointed without moving the detection hardware, which is necessary for laboratory and ground-based field demonstrations of the breadboard system. Light from the fiber is collimated and passed through the filter section to isolate a narrow portion of the spectrum around a single absorption line. The filter section consists of one or two tilt-tunable custom bandpass filters with a full width at half maximum (FWHM) of 0.1 nm. Additional filtering, such as an air-spaced or solid etalon, also can be accommodated. The filters reduce extraneous light from entering the interferometer, which could wash out the interference pattern or add stray light at the detector. Sharp filters dramatically reduce the light throughput, but allow for increased OPD (since the coherence length increases), and improved sensitivity to shifts in absorption lines.

The interferometer is aligned so that the two emerging light beams interfere at a small angle with respect to each other, which creates a fringe pattern with the fringe wavevector aligned along the long axis of the CCD array. The CCD records the interference fringes, and the Doppler shift in the incident light spectrum is converted to a phase shift in the fringe pattern. As indicated above, this phase shift is relatively small, but easily detected provided that the noise is low enough. In practice, the sensitivity is limited by several technical challenges, including the SNR, wavefront error from imperfect optics, thermal drift, vibrations, and time-varying source and filter functions. These issues are being addressed during the breadboard phase of the project.

To minimize disturbances from air currents, the interferometer is sealed in a chamber that consists of two aluminum shells separated by multi-layer thermal insulation. Light enters and exits the interferometer through anti-reflection coated windows. Thermistors are used to monitor the temperature inside the inner shell. Interferometer beam alignment and changes in the OPD are performed through computer control.

Initial breadboard testing was directed at assessing and improving the stability of the interferometer. Preliminary data were obtained using a stabilized HeNe laser without the filter set to measure the relative interferometer phase of the laser line as a function of time. Data for a two-minute experiment were fit to a straight line, which gave a rate for the phase drift of -0.0003 rad/s. This slope corresponds to a wind speed equivalent Doppler shift (EDS) of 3.9 m/s per second (*i.e.,* the instrumental phase drift per second is equivalent to the Doppler shift that would be observed for a 3.9-m/s wind speed). Thermistor measurements inside the interferometer chamber indicated a steady increase in temperature of +0.00012 K/s during the experiment. Based on the thermal expansion characteristics of the relevant components, this temperature increase accounted for approximately half of the phase drift and underscores the need for a thermally stable engineering model. The root mean square (RMS) of the residuals for the line fit corresponds to a wind speed EDS noise of 0.7 m/s per second. When the filters are added to the optics train, the system stability will be further reduced as a result of drifts in the filter characteristics. The sources of the phase drift and residuals, other than thermal instability, have not been determined, but likely are due to pointing jitter or error in the optical components. The preliminary data indicate that an integration time of roughly one second would be sufficient to discern a wind speed near 10 m/s with an error of several m/s. This level of performance is adequate for the purposes of the breadboard, but will be unsuitable for use in limb wind detection, where up to 100 seconds of integration time could be required.

To monitor system stability, a metrology source will be incorporated as a reference. The metrology subsystem will consist of a laser stabilized to the bottom dip of the oxygen line to be measured. The metrology laser will follow a path through the filters to the interferometer and interfere at the CCD with precisely the same wavelength and geometrical field of view as the light to be measured. With the laser stabilized to an oxygen line standard, the $1/f$ noise in the laser

frequency spectrum is eliminated so any fringe drift at the CCD can be directly calibrated. By alternating CCD views between the measurement source and the metrology laser, it is estimated that the interferometer drift can be reduced by one to two orders of magnitude. The next largest source of instability is in the filter section, since extraneous tilts or temperature changes will result in small, but measurable changes in the observed spectrum. The metrology laser also could be coupled with an auto-balance receiver and proportional integral derivative (PID) control in a feedback loop to maintain proper orientation of the filters for maximum transmission of the laser line. However, this approach would add complexity and might not be required to achieve the objectives of this project.

The measurement scheme must be able to separate variations in the wind speed from the interferometer drift/noise. This requirement can be achieved by keeping the integration time for each measurement short enough that the passive drift in the interferometer phase is minimal. The metrology laser can be used to null the system after each measurement so that variations between measurements can be attributed to variations in wind speed. The current stability of the breadboard system dictates that the measurement integration time is only on the order of one second; therefore, to achieve an adequate SNR with this approach, the source used for demonstrating the breadboard system must be very bright. An alternative method to accumulate sufficient SNR is to rapidly interleave measurements from the source and the metrology laser. The source data could be binned and added to achieve a longer effective integration time, and the instrument phase drift could be corrected using a calibration constructed from the metrology data. This method is limited by CCD readout noise.

Once the breadboard metrology subsystem is completed, laboratory tests will be conducted to demonstrate the ability to detect small instrument phase shifts and correct for instrument drift and noise. The light source will be a fiber-coupled light-emitting diode centered at 780 nm with a 50-nm bandwidth. This source provides 2 mW of power exiting the fiber and up to 1 μW of power through the 0.1-nm narrow band filter. For simplicity, initial testing will be performed by observing one of the deepest oxygen absorbance lines in the A-band at two different optical path lengths. By rapidly alternating between a long and short path, the depth of the absorbance line feature in the filter band pass (Fig. 4) will vary between deep and shallow. Although this approach is different from a frequency shift in the line center, it will affect the observed instrument phase in a similar way and is easier to implement in the laboratory than an actual Doppler shift. The metrology laser subsystem then will be employed to determine and demonstrate a reduction in instrument drift and noise.

Field measurements will be performed from a roof-top observation deck at Ball Aerospace & Technologies Corp. To obtain an adequate signal under ground-based conditions, the fiber-coupled telescope will be programmed to track near the solar disk with the Sun moving toward the horizon. The measurement objective will be to clearly distinguish wind-induced phase shifts from instrumental drift and noise, and to correlate the interferometer data with an independent wind speed sensor.

Knowledge gained from breadboard phase of this project, as well as the radiometric and instrument modeling efforts described below, will be used to develop an engineering model design that is thermally and mechanically stable and achieves the best compromise in line selection, filtering approach, and OPD. The goal for stability will be to increase the time for an acceptable drift by roughly two orders of magnitude and decrease the noise by a factor of 10 relative to the breadboard system. The strategy will be to construct a small solid-block interferometer composed of fused silica, Zerodur® or ULE®, with wedged Zerodur® or ULE® spacers to provide a fixed OPD and wavefront tilt. Thermal, vibration, and acoustic insulation also will be used and an etalon filter will be included in the thermal housing. Thermal stability maintained at ±1 mK over 100 seconds is attainable and would produce only 0.03 m/s of EDS. It is expected that the noise level (residuals about the drift) also will drop since the tilt, torsional motion, and vibrations will be minimized. The need for a metrology laser in the engineering model will depend on the overall stability of the interferometer/filter/optical system. If a metrology laser is required, the interleave time could be increased to 100 seconds, which would permit practical implementation with actual wind sources.

IV. Radiative Transfer Model and Wind Speed Retrieval

A radiative transfer model is under development in support of the instrument trade studies. The model computes interferograms and wind-induced phase shifts, which depend on the atmospheric state, viewing geometry, and sensor configuration. The theoretical background is derived from the work of Hays and Abreu [5] and adopts a single-scattering approximation. Knowledge of the phase shift and measurement noise provides a basis for retrieval simulations, which estimate errors on retrieved layer wind speeds. The retrieval scheme is based on an optimal estimation approach [6].

The primary goal for the combined radiative transfer and retrieval models is to identify the optimal configuration of the following system parameters: (1) the specific A-band absorption line or lines used in the measurement, (2) the filter function and spectral position over the absorbance line or lines, and (3) the interferometer OPD. These parameters must be optimized to best meet the science and measurement objectives within the technology limitations of the hardware. For example, the system components and stability will limit the achievable SNR, and it is not technically possible to fabricate a filter with an ideal filter function. A secondary goal is to determine the sensitivity of the measurement to

atmospheric conditions, including variations in viewing geometry, *a priori* knowledge of the approximate layer wind speed, surface albedo, atmospheric pressure, temperature, aerosols, and clouds. Knowledge gained from the models will facilitate development of test-flight and on-orbit operation concepts and calibration methodology.

The details of the model are beyond the scope of this paper; however, preliminary results indicate that the optimum instrument parameters change significantly as a function of the line-of-sight viewing altitude in the limb. Within the oxygen A-band, the lower frequency lines are more sensitive to wind speed in the lower part of the troposphere; whereas, the higher frequency lines are mores sensitive in the stratosphere. Specifically, for a given wind speed the greatest Doppler shift at an altitude of 2 km occurs for the absorbance line near 12,954 cm^{-1}, and at an altitude of 20 km, the greatest Doppler shift is observed for the line near 13,000 cm^{-1}. Additionally, the apparent width of the spectral features decreases with increasing limb altitude, which increases the optimum interferometer OPD. For a given absorbance line, the optimum interferometer OPD increases from less than 1 cm at a 2-km limb height to several cm at a 20-km limb height. Initial wind retrieval calculations on simulated data indicate that the measurement sensitivity is greatest in the mid troposphere and peaks at a limb height of about 7 km. The error in the wind retrieval in this region is on the order of 2 to 3 m/s, but can be near 7 m/s at the bottom and top of the troposphere. The difference in wind error as a function of the instrument parameters can be as high as 4 m/s depending on the viewing location in the limb. These preliminary calculations emphasize that the instrument parameters must be carefully selected to meet the measurement requirements for a space-based platform.

V. Instrument Model Development

An instrument system model is being developed to help predict and evaluate the performance of the Michelson interferometer and to assess the results from the laboratory experiments. A key purpose of the model is to predict the ability of the instrument to detect small phase shifts in the presence of noise sources, which are generated in the model using a Monte Carlo simulation. The instrument phase shift is related to the wind speed using the radiative transfer model discussed previously. The input for the instrument model is the absorption spectra of the P-branch of the oxygen A-band, including radiance estimates. The model tracks the signal from the sunlight scattered off the atmosphere (or laboratory source), through the chosen oxygen A-band absorption line, then adds the Doppler shift due to the wind speed of the atmosphere, and continues the signal through the optical filters and Michelson interferometer.

The optical filters can include narrow-band filters, a solid etalon, or adjustable Fabry-Perot filters. The optical filter transmission shape and wavelength position with respect to the absorption line pair (centered on a single line, on a single line edge, or centered between the Doublet pair) is an input, along with the interferometer OPD and the resulting fringe modulation intensity. Trade studies are being performed on the tolerances and stability of optical filters, interferometer optics, and detection. Calibration errors are included as needed.

The detection model includes noise expressed in terms of SNR of individual samples of the fringe pattern on the detector. Two SNRs are defined, one relative to the average background radiance, and the other relative to the fringe modulation: SNR ≡ (background radiance)/(total noise) and SNR_{fringe} ≡ (fringe modulation)/(noise on fringe). The detector noise in the detector model can include dark current fluctuations, read noise, photon noise and digitization noise, and can be expressed as a single SNR. Trades can be done on samples per fringe period, integration time, noise on each sample, and the effect of binning multiple detector elements.

The phase is estimated by data reduction of the samples of the fringe pattern on the CCD detector. A least-squares fit is implemented to obtain the best fit of the fringe data to a sine wave of a given frequency and phase shift. Monte Carlo estimates of the phase shift fit error from the curve fit sine wave can be performed as a function of SNR of each sample, number of fringe periods and samples over the fringe period, as well as tolerances and calibration errors.

An example of the sampling over two periods with eight samples is shown at the top of Fig. 8. The statistical distribution of errors from the Monte Carlo run of 2000 cases allows for random sample alignment of the fringe with-respect-to the samples. The result shown at the bottom of Fig. 8 gives a standard deviation of 0.0021 fringe for a sample SNR of 353 with a peak modulation of 20%. For the same error at 10% modulation, the noise also must be reduced by one half. A principal conclusion of the Monte Carlo trades on phase error estimates is that a significant number of samples across the interference pattern on the CCD, perhaps eight to 32, might produce smaller errors in the phase estimate even though each sample may have lower SNR than with a smaller number of samples.

VI. Conclusions

The unique challenges for PAWS compared to other interferometer Doppler wind sensors are that (1) an absorption line rather than an emission line is being measured, and (2) the measurement is targeting the troposphere. These conditions complicate the measurement and result in a significant dependence of the optimal instrument parameters on the viewing tangent height within the limb. To maintain simplicity, an instrument design is being pursued that achieves a good compromise for line selection, filtering approach, and OPD. Additionally, initial testing of the breadboard instrument emphasized the need for high thermal and mechanical stability and indicated that a metrology subsystem might be required to separate the signal from instrumental drift.

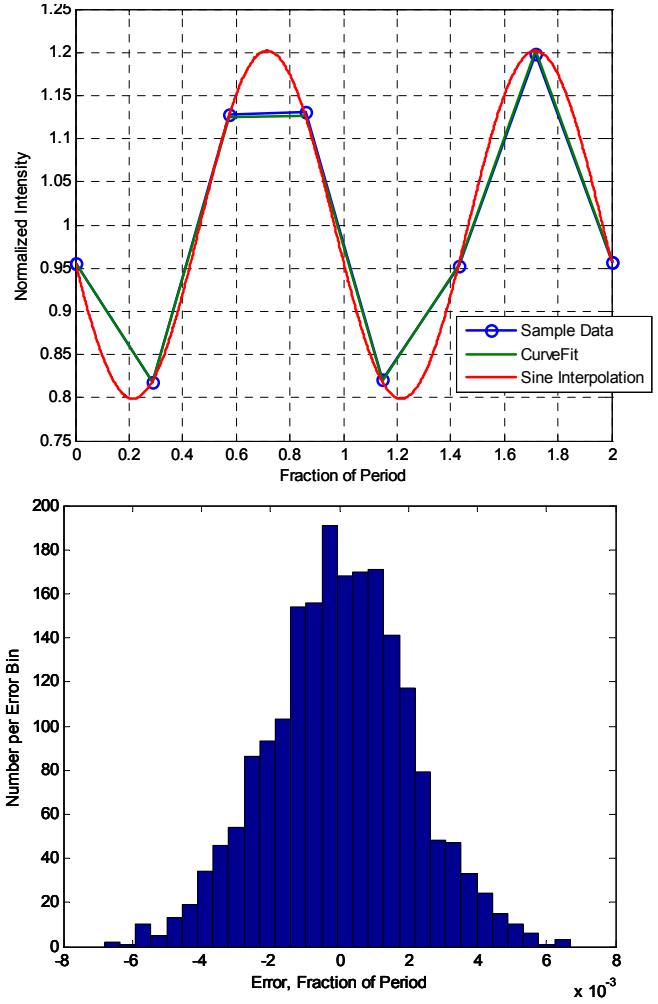

Fig. 8. Interferogram sampling approach showing eight points over two periods (top). Statistical distribution of errors for a Monte Carlo run with 2000 cases.

ACKNOWLEDGMENTS

We gratefully acknowledge the support of NASA ESTO, and our COTR, Janice Buckner. This project is funded by NASA ESTO Contract NNG06HX07C.

REFERENCES

[1] "Earth science and applications from space: National imperatives for the next decade and beyond." The National Academies Press, Washington, DC, 2007.

[2] G.G. Shepherd, G. Thuillier, W.A. Gault, B.H. Solheim, C. Hersom, J.M. Alunni, J.-F. Brun, S. Brune, P. Charlot, L.L. Cogger, D.-L. Desaulniers, W.F.J. Evans, R.L. Gattinger, F. Girod, D. Harvie, R.H. Hum, D.J.W. Kendall, E.J. Llewellyn, R.P. Lowe, J. Ohrt, F. Pasternak, O. Peillet, I. Powell, Y. Rochon, W.E. Ward, R.H. Wiens, and J. Wimperis, "WINDII, the wind imaging interferometer on the Upper Atmosphere Research Satellite," *J. Geophys. Res.*, vol. 98, pp. 10725-10750, June 1993.

[3] L.R. Brown and C. Plymate, "Experimental line parameters of the oxygen A-band at 760 nm." *J. Mol. Spec.*, vol. 199, pp. 166-179, 2000.

[4] P. Rahnama, Y.J. Rochon, I.C. McDade, G.G. Shepherd, W.A. Gault, and A. Scott, "Satellite measurement of stratospheric winds and ozone using Doppler Michelson interferometry. Part I: instrument model and measurement simulation," *J. Atmos. Oceanic Tech.*, vol. 23, pp. 753-769, June 2006.

[5] P. B. Hays and V. J. Abreu, "Absorption line profiles in a moving atmosphere: a single scattering linear perturbation theory." *J. Geophys. Res.*, vol. 94, pp. 18351-18365, 1989.

[6] C. D. Rodgers, "Inverse methods for atmospheric sounding: theory and practice," *Series on Atmospheric, Oceanic and Planetary Physics*, vol. l2, World Scientific Publishing Co., 2000.